https://doi.org/10.1016/j.actamat.2019.09.044

Dissecting the influence of nanoscale concentration modulation on martensitic transformation in multifunctional alloys

Jiaming Zhu [1], Hong-Hui Wu [6], Xu-Sheng Yang [2,3], He Huang [6], Tong-Yi Zhang [5,*], Yunzhi Wang [4,*], San-Qiang Shi [1,*]

[1] Department of Mechanical Engineering, The Hong Kong Polytechnic University, Hong Kong, China

[2] Advanced Manufacturing Technology Research Centre, Department of Industrial and Systems Engineering, The Hong Kong Polytechnic University, Hung Hom, Kowloon, Hong Kong, China

[3] Hong Kong Polytechnic University Shenzhen Research Institute, Shenzhen 518057, China

[4] Department of Materials Science and Engineering, The Ohio State University, 2041 College Road, Columbus, OH 43210, USA

[5] Shanghai University Materials Genome Institute and Shanghai Materials Genome Institute, Shanghai University, 99 Shangda Road, Shanghai 200444, China

[6] Beijing advanced innovation center for materials genome engineering, State Key Laboratory for Advanced Metals and Materials, University of Science and Technology Beijing, Beijing 100083, China

Abstract

Nanoscale concentration modulation (CM) is a novel and effective approach of manipulating martensitic transformations (MTs) for developing next-generation high-performance shape memory alloys (SMAs). Spinodal decomposition is one of the most economic methods to obtain bulk compositionally modulated materials for practical applications. The wavelength, amplitude, and statistical distribution of CM generated by spinodal decomposition are tunable via adjusting the ageing temperature, or the ageing time. However, how these features influence the effect of CM on MTs still remains largely unexplored. In this study, theoretical analyses and computer simulations are combined to dissect the influence of these features on the kinetic process of MTs and mechanical properties of SMAs. The findings of this study provide insights and guidance on the design of SMAs for desired mechanical properties via CM engineering. Moreover, the findings are applicable to not only SMAs but also other materials that have MTs, e.g. steels and high-entropy alloys.

Keywords: Concentration modulation, Martensitic transformation, Shape memory alloy, Nucleation, Spinodal decomposition

1. Introduction

Understanding and manipulating the kinetic process of martensitic transformations (MTs) are of both fundamental and technological significance for developing advanced materials. For example, a metal composite (i.e. the NICSMA [1]) with large elastic strain limit and a high entropy dual-phase alloy overcoming the strength and ductility trade-off [2] are developed by making the otherwise sharp stress-induced MTs occuring over an extended deformation range. Moreover, shape memory alloys (SMAs) with low modulus, reduced hysteresis, or linear superelasticity are also designed via tuning the MT process through defect engineering [3,4], composition adjustment [5–7], nanocrystallization [8,9], or the synergic effect between nanoscale concentration modulation (CM) and pre-straining [10]. These properties are desired in applications such as orthopedic implants [11], high efficiency actuators [12], active medical catheters [13], and environmental friendly cooling devices [14,15], etc. Therefore, an effective approach that allows manipulating MT will strongly support the development of high-performance structural and functional materials.

The strategy that making MTs change from first-order to continuous is widely adopted when manipulating the kinetic process of MTs. Strain glass transition [16], which transforms a sharp MT to a continuous phase transition, represents a progress in this direction. But it is still difficult to achieve non-hysteretic and linear-superelastic stress-strain response with ultralow modulus. Recently, a novel approach, nanoscale CM, has been demonstrated as a general and effective approach of tailoring MTs [17]. In sharp contrast to the strain glass transition, which uses local stress to break the long-term ordering of strain and thus no internally twinned martensitic patterns exist, the nanoscale CM approach retains the long-term strain order of martensitic domains and generates self-accommodating morphologies. In particular, it has been reported that a combination of unprecedented properties can be achieved by designing the transformation pathway of martensites via adjusting the CM in SMAs [10].

Spinodal decomposition, as one of the most economic methods to fabricate bulk compositionally modulated materials for practical applications, is powerful in engineering nanoscale CMs in materials. In fact, CMs induced by spinodal decomposition are observed in many SMAs, such as TiNb [18,19], MnCu [20,21], FeMn [22] alloys, to name a few. It should be pointed out that CMs generated by spinodal decomposition varies in wavelength, amplitude, and concentration profile shape according to the ageing temperature and ageing time. For instance, the wavelength is a function of the ageing temperature, the amplitude gradually increases at the early stage of spinodal decomposition, and the concentration profile changes from a sinusoidal-like shape to a square-

like shape as the ageing time extends. However, how these features of CM influence the nucleation and growth process of martensites and mechanical properties of SMAs still remains unknown, impeding the design of materials with desired mechanical properties via CM engineering.

In this study, stress-induced MTs and mechanical properties of systems with representative CMs generated from spinodal decomposition are systematically investigated by a combination of theoretical analyses and computer simulations. In particular, thermodynamic analyses are performed to characterize the influence of CM on the nucleation of martensites. Then phase field simulations are designed to dissect the influence of CM wavelength, CM amplitude, and concentration profile shape on the kinetic process of MTs and mechanical properties of materials. A good agreement is reached between the theoretical analyses and phase field simulation results. It is expected that mechanical properties of materials could be tailored by adjusting CM wavelength, CM amplitude, and concentration profile shape, e.g. critical stress of MT, transformation hysteresis, and the linearity of stress strain (SS) curves. Below we will first briefly introduce the phase field model developed, followed by simulation results of representative systems throughout spinodal decomposition process in Section 3. The influence of wavelength, amplitude, and concentration profile shape on MT and mechanical properties are discussed in Section 4. Major findings are summarized in Section 5.

2. Phase field model

It is reported that a CM of Nb, between 8 at.% and 20 at.%, induced by spinodal decomposition is observed in a multifunctional β TiNb-base alloy, Ti2448 (short for Ti-24Nb-4Zr-8Sn-0.1O in wt.%) [23]. This CM exihibits strong influence on both the stress- and thermally-induced MT in Ti2448 due to the concentration dependence of phase stability of the parent and martensitic phases [17,23]. It is well known that MT is a diffusionless phase transition, decoupling it from the concentration evolution process, which means the concentration evolution and MT can be treated individually. Based on this fact, we first create compositionally modulated systems via spinodal decomposition at 773K, then uniaxial loading is applied on these systems at 300K to investigate the evolution of stress-induced MT and mechanical properties of materials.

The MT in Ti2448 is from the β parent phase (BCC, point group $m\bar{3}m$) to the α'' martensite (orthorhombic, point group *mmm*) [24,25]. The symmetry breaking associated to this MT generates six martensitic variants. In our phase field model, the parent and martensitic phases are characterized by using six non-conserved structural order parameters, η_p (p=1~6), with

$(\eta_{p=1\sim6} = 0)$ representing the parent phase and $(\eta_p = \pm 1,\ \eta_{q=1\sim6,q\neq p} = 0)$ representing the *p*-th correspondence variant of the martensitic phase, where +1 and -1 denote atomic shuffles in two opposite directions in a correspondence variant. The three-dimensional (3D) phase field model is formulated based on the Landau theory [26], the gradient thermodynamics [27,28], and the modified Khachaturyan–Shatalov's microelasticity theory (KS theory) [17,29,30] of structural phase transformations. The concentration variation during spinodal decomposition is governed by the Cahn-Hilliard equation [31], and the temporal and spatial evolution of the structural order parameters during MT are described by the time-dependent Ginzburg-Landau equation [32]. It should be pointed out that the concentration dependence of Landau free energy is considered in this phase field model to characterize the influence of CM on MT, as Fig. 1(a) shows. The expansion coefficients in the Landau free energy for the MT and in the chemical free energy of the parent phase for spinodal decomposition are validated by quantitative comparison between simulation results and corresponding experimental reports. Details on the development and validation of the phase field model are available in literature [17]. The system size used in the simulations is 128 nm×128 nm×128 nm. Periodical boundary conditions are applied along all three dimensions.

3. Simulation results

3.1 Evolution of concentration modulation during spinodal decomposition

As it is known, spinodal decomposition occurs via concentration fluctuations that are infinitesimal in degree but large in extent [31]. To characterize the evolution of the CM in terms of its wavelength and amplitude during the spinodal decomposition, 3D phase field simulations are performed for isothermal ageing of a compositionally uniform system at 773K. The results are shown in Fig. 2(i)-(p), with 1D concentration profiles along the body-diagonal of the 3D system aged for different times plotted in Figure 1(b) that show quantitatively the time-evolution of the amplitude and wavelength of the CM. It is readily seen that the amplitude of the CM gradually increases until the equilibrium concentrations are reached. Moreover, Fig. 1(b) demonstrates that the CM wavelength changes with ageing time as well. It is interesting to note that CM wavelength has no obviously change before concentration reaches equilibrium concentrations (see t^*=0-1380 in Fig. 1(b)). After that, however, CM wavelength increases via coarsening process (see t^*=1900-7100 in Fig. 1(b)). With the proceed of coarsening, the shape of 1D concentration profile changes from sinusoidal-like to square-like as demonstrated in Fig. 1(b). It should be pointed out that results that are similar to those shown in Fig. 1 have been reported in literatures [10] and [17].

Here we conduct a more detailed analysis on the CM, in terms of amplitude, wavelength, and concentration profile shape, and its influence on the SS curve to demonstrate the significance of these aspects and to provide guidance to experiments.

Accompanying the evolution of amplitude, wavelength, and concentration profile shape, the statistical distribution of concentration (SDC) keeps changing throughout the spinodal decomposition process as shown in Fig. 1(c), serving as another parameter to characterize the CM. Figure 1(c) indicates that the concentration range first gradually expands as the CM amplitude increases, followed by the change of volume ratio among different concentrations with a trend of improving the volume fraction of equilibrium concentrations (8 at.% and 20 at.%) at the expense of initial average concentration (15 at.%). In general, the SDC can be categorized into two types: one is n-type whose volume fraction peaks at the vicinity of initial average concentration (see t^*=1100 and t^*=1240 in Fig. 1(c)); another is u-type whose volume fraction close to equilibrium concentrations is larger than that of the average concentration (see t^*=1900 and t^*=7100 in Fig. 1(c)).

The analyses in this section demonstrate that the complex CM generated by spinodal decomposition can be well described by parameters including amplitude, wavelength, concentration profile shape, and SDC. As will be shown below, these parameters influence not only the kinetic process of the MT but also the mechanical properties of the system.

3.2 MT and mechanical properties of systems with different CMs

Figure 2 and 3 show the microstructure evolution during stress-induced MT in systems aged for different time upon loading and unloading process, respectively. Corresponding SS curves are plotted in Fig. 1(d). Figure 2(a)-(h) demonstrate that the forward MT starts at lower stress level and occurs over a larger stress range as CM develops (see Fig. 2(i)-(p)). Moreover, in response to the extension of ageing time, the backward MT initiates from a higher stress level and happens over an extended stress range as shown in Fig. 3. However, for the system shown in Fig. 2(h) and 3(h), a considerable amount of martensites appear at the beginning of forward MT and survive even when the system is completely unloaded. These phenomena are consistent with what we observed in the SS curves shown in Fig. 1(d): (i) SS curve deviates from linear at lower stress levels during loading as the ageing time increases because the forward MT occurs and contributes to deformation at lower stress levels; (ii) the stress plateaus upon loading and unloading gradually disappear as CM develops due to the change of MT from avalanche-like (which is a typical feature of conventional first-order MT) to macroscopically continuous; (iii) a small stress plateau

reemerges at low stress level in the system aged for t^*=7100 because the confinement of CM on the nucleation of martensite changes as the concentration profile shape and the SDC evolve.

4. Discussion

4.1 Characterizing the influence of CM on nucleation of martensite

The work of Olson and Cohen [33,34] demonstrates that the nucleation of martensites can be analyzed via the classical nucleation theory. The free energy change associated with the formation of a martensitic nucleus reads

$$\Delta F = \int_V \left[\Delta f_{\mathrm{ch}}(\boldsymbol{r}) + \frac{1}{2}\sigma_{\mathrm{ij}}(\boldsymbol{r})\varepsilon_{\mathrm{ij}}(\boldsymbol{r})\right] dV + \int_S \gamma_0(\boldsymbol{r}) dS \tag{1}$$

where V is the space occupied by the nucleus, S the surface of the nucleus, $\boldsymbol{r}$ the position vector. Δf_{ch} designates the chemical driving force of MT. $\sigma_{\mathrm{ij}}(\boldsymbol{r})$ and $\varepsilon_{\mathrm{ij}}(\boldsymbol{r})$ represent local stress and local strain induced by this nucleus in materials. $\gamma_0(\boldsymbol{r})$ is the interfacial energy. Equation (1) indicates that CM could influence the nucleation of martensite via changing the chemical free energy, the coherency elastic strain energy, the interfacial energy, or all of them. While it has been demonstrated that the composition dependence of MTs mainly originated from the dependence of chemical free energy on composition [35]. Therefore, the influence of CM on the nucleation of martensite can be estimated via comparing the chemical driving force before and after introducing CM. In a compositionally uniform (CU) system, the chemical driving force reads $\Delta F_{\mathrm{ch}}^{\mathrm{U}} = 4\pi \int_0^{R_{\mathrm{U}}} \Delta f_{\mathrm{ch}}^{\mathrm{U}} \rho^2 d\rho$, where $\Delta f_{\mathrm{ch}}^{\mathrm{U}}$ is the MT driving force density of the CU system, R_{U} denotes the critical nucleation radius of martensites of the CU system, and ρ is the radial distance in a spherical coordinate system. Note that, for simplicity, the martensitic nucleus is assumed to be a sphere as suggested by Olson and Cohen [33]. After introducing CM into the CU system without changing its average composition, the chemical driving force in a sphere region with a radius of R_{U} is calculated as $\Delta F_{\mathrm{ch}}^{\mathrm{CM}} = 4\pi \int_0^{R_{\mathrm{U}}} \Delta f_{\mathrm{ch}}(\rho) \rho^2 d\rho$. Then the following parameter can be used to estimate the influence of CM on the nucleation of martensite

$$\Psi = \Delta F_{\mathrm{ch}}^{\mathrm{CM}} - \Delta F_{\mathrm{ch}}^{\mathrm{U}} = 4\pi \int_0^{R_{\mathrm{U}}} \left[\Delta f_{\mathrm{ch}}(\rho) - \Delta f_{\mathrm{ch}}^{\mathrm{U}}\right] \rho^2 d\rho. \tag{2}$$

It is conceivable that the value of Ψ is a function of CM, in terms of wavelength, amplitude, and concentration profile shape, because Δf_{ch} is dictated by the concentration distribution in the sphere over which the integration is performed as Fig. 4(a)-(c) show. Moreover, Figure 1(b) indicates that CMs generated from spinodal decomposition can be described by a sinusoidal curve

or a square curve. Therefore, Figure 4(d) shows the variation of Ψ with wavelength for CMs possessing different amplitudes and concentration profile shapes. It is readily seen that sinusoidal CMs with larger wavelength contribute a larger driving force (more negative $\Delta F_{\mathrm{ch}}^{\mathrm{CM}}$ and Ψ) to the nucleation of martensites. In particular, Ψ first drops rapidly and then declines slowly with the increase of wavelength. The critical wavelength separating the fast- and slow-stage is $5.9R_{\mathrm{U}}$, regardless of the amplitude. The R_{U} is ~3nm in this study which is consistent with theoretical estimations [36,37]. Similar phenomenon is also observed in the square CM, but the critical wavelength of square CMs is $4R_{\mathrm{U}}$, and Ψ remains unchanged when wavelength is larger than this value. Moreover, comparison among sinusoidal CMs of different amplitudes implies that CMs with larger amplitude provide larger driving force for the nucleation of martensites. To validate these theoretical analyses and reveal the influence of CM on mechanical properties, phase field simulations are performed in following sections.

4.2 Influence of CM wavelength on MT and mechanical properties

Figure 5(a) shows systems with five different average CM wavelengths L=9~110 nm generated from spinodal decomposition, which can be realized easily in experiment by controlling the ageing temperature. Note that the average CM wavelengths of these systems are determined by the linear intercept method. Figure 5(b) and 5(c) indicate that all of these computational cells have a sinusoidal-like concentration profile and have almost the same SDC (CM amplitude), respectively, which excludes the influence of amplitude and concentration profile shape on MTs and mechanical properties. The microstructure evolution process of these systems during MT upon loading and unloading are presented in Fig. 6. In consistent with our theoretical prediction, the influence of CM on the kinetic process of MT becomes more and more apparent as CM wavelength increases, e.g. MT initiates at a lower stress level and occurs over a larger stress range in systems with a larger CM wavelength. To reveal how CM wavelength affect the nucleation of martensites, the chemical driving force of these systems are plotted in Fig. 7(a). It is readily seen that the nucleation sites (regions with negative Δf_{ch}) in Fig. 7(a3)-(a5) is much larger than those in Fig. 7(a1) and 7(a2), providing a larger driving force for martensites to nucleate and thus lowering the critical stress of MT (σ_{Ms}) as observed in Fig. 6. Corresponding to the change of MT, the SS curve gradually transforms from a square-like one to slim ones as Fig. 7(b) shows. Quantitative analyses performed on these SS curves (see Fig. 8) demonstrate that the influence of CM on mechanical properties, in terms of $\sigma_{\mathrm{M_s}}$ and hysteresis, can be divide into two stages: when L<15 nm, $\sigma_{\mathrm{M_s}}$ and hysteresis are strong functions of CM wavelength; while their dependence on CM wavelength becomes much weaker when L>15 nm. This phenomenon agrees very well with

our theoretical analysis shown in Fig. 4(d) which predicts a critical CM wavelength of ~18 nm for the influence of CM on MT. In addition, Fig. 6 demonstrates that austenite and martensite coexist at the end/initial of the loading/unloading process and that the retained martensitic domains still exist in a system even the external load is completely removed. This makes it difficult to define the martensite finish stress, austenite start stress, and austenite finish stress.

4.3 Influence of CM amplitude on MT and mechanical properties

Figure 1(b) demonstrates that CM mainly varies in amplitude without obvious change in wavelength within the ageing time of t^*=1320. This is consistent with both the theory of spinodal decomposition [31] and experimental observations [19]. During spinodal decomposition, the growth rate of concentration fluctuations is a function of their wavelengths. The observed CM at the early stage of spinodal decomposition corresponds to the wavelength that has the highest growth rate. Therefore, the CM wavelength does not change obviously at the early stage of spinodal decomposition. Then it is reasonable to relate the change of MT shown in Fig. 2(a)-(f) and 3(a)-(f) and the evolution of mechanical properties shown in Fig. 1(d) to the variation of CM amplitude. The growth of CM amplitude during spinodal decomposition is presented in Fig. 9 which shows that Nb becomes leaner and richer at Nb-lean and Nb-rich regions, respectively, via spreading over a larger concentration range as CM develops. Because the phase stability of the parent and martensitic phase are concentration dependent (see Fig. 1(a)), an enhanced CM amplitude strengthens the difference in phase stability between Nb-lean and Nb-rich regions, broadening the phase stability spectrum of the system as Fig. 9(f)-(j) shows. With a more broadened phase stability spectrum in the system, the MT becomes more gradual as observed in Fig. 2(a)-(f) and 3(a)-(f), which indicates that CM becomes more effective in transforming the otherwise sharp MT into macroscopically continuous one. Moreover, the more gradual MT process implies a stronger regulation effect of CM on the growth of martensitic domains. As a consequence, a lower $\sigma_{\mathrm{M_s}}$ and a smaller hysteresis could be obtained as shown in Fig. 1(d) and 10. In addition, Fig. 10 demonstrates that the influence of CM on MTs and mechanical properties is in proportion to its amplitude. This is consistent with the prediction of Fig. 4(d).

4.4 Influence of concentration profile shape on MT and mechanical properties

Figure 1(b) indicates that the concentration profile changes from sinusoidal-like to square-like as spinodal decomposition proceeds. Concomitantly, the SDC transforms from the n-type to the u-type as mentioned earlier. The concentration dependence of phase stability of the parent and martensitic phase makes the σ_{Ms} a function of concentration as Fig. 11 shows. Therefore, the SDC

(the concentration profile) dictates the volume of a system that transforms into martensitic phase at a certain stress level (see Fig. 11) and thus determines the mechanical response of the system to external loads. For example, Fig. 1(c) demonstrates that the system shown in Fig. 2(h) and 3(h) distinguishes itself from other systems by having a u-type SDC, which implies that a large volume fraction of the system will engage in MT at a low stress level as demonstrated in Fig. 2(h). The sudden appearance of considerable martensite, in turn, leads to a strain jump on the SS curve plotted in Fig. 1(d). In fact, SS curves of u-type SDCs always show a strain jump, which is quite different from those of n-type SDCs (compare Fig. 7(b2)-(b5) with 12(c)).

Moreover, different from the case in an n-type SDC, the intermediate concentrations in the u-type SDC are partially depleted as Fig. 11 shows, which means only limited volume of the system will further transforms into martensite after the initiation of MT. Therefore, the evolution of martensitic domains in systems with a u-type SDC is not as obvious as that in systems with an n-type SDC, which can be readily seen by comparing Fig. 2(h) and 3(h) with Fig. 2(c)-(g) and 3(c)-(g), respectively.

In addition, Fig. 4(d) demonstrates that a square CM contributes a larger driving force to MT than a sinusoidal CM when they have the same wavelength and amplitude. To test this prediction, systems with square-like CMs (u-type SDC) of different wavelengths are investigated as Fig. 12 shows. It is readily seen that all SS curves of these system show a strain jump which implies the initiation of MT. As compared with systems that have an equal wavelength but different concentration profile shape, these systems have a lower $\sigma_{\mathrm{M_s}}$ (compare Fig. 13 with Fig. 8). This indicates that these square-like CMs do have a larger driving force of MT than those sinusoidal-like CMs although they have the same wavelength and amplitude. Note that a larger driving force of MT means a lower free energy of martensites. Then it is natural to expect that Nb-lean regions should be able to accommodate retained martensites if their driving force of MT are large enough. Figure 3(h) and 6(j) demonstrate that this assumption holds for both square-like and sinusoidal-like CM. It should be noted that Fig. 4(d) indicates that the $\sigma_{\mathrm{M_s}}$ of square CMs should be CM wavelength independent when the wavelength is larger than the critical wavelength $4R_{\mathrm{U}}$ (~12 nm); however, the $\sigma_{\mathrm{M_s}}$ shown in Fig. 13 evolves with CM wavelength. This is because CMs of systems shown in Fig. 12 are square-like CMs instead of ideal square CMs.

5. Conclusion

The influence of nanoscale concentration modulation (CM) on martensitic transformation (MT) and mechanical properties of a multifunctional β TiNb-base shape memory alloy are

systematically studied via thermodynamic analyses and phase field simulations. Theoretical analyses agree with phase field simulation results very well. The major findings are as follows:

(i) A thermodynamic parameter Ψ, which characterizes the change of chemical driving force of MT accompanying the introduction of CM, is defined to estimate the influence of CMs on the nucleation of martensites. It is found that the chemical driving force of MT increases linearly as CM amplitude grows. While it rises rapidly at first then slowly as CM wavelength increases. The critical wavelength separating these two stages is dependent on concentration profile shape , not on CM amplitude.

(ii) CMs with a larger wavelength make stress-induced MTs initiate at a lower stress level and occur over a larger stress range, generating stress strain curves with reduced critical stress of MT ($\sigma_{\mathrm{M_s}}$) and diminished hysteresis.

(iii) CM amplitude dictates the width of phase stability spectrum and thus determines the stress range of MT. CMs with a larger CM amplitude are more effective in transforming sharp MTs into macroscopically continuous ones.

(iv) The shape of concentration profile controls the statistical distribution of concentration that determines the volume fraction of MT at a certain stress level, which influences the stress strain curve.

The findings of this study are expected to shed light on fundamental understanding of the influence of CM on MTs and provide guidance to practical designs of CM in materials for desired mechanical properties. Moreover, these findings are applicable to not only MTs in shape memory alloys but also MTs in other materials such as steels and high-entropy alloys.

Acknowledgement

TYZ acknowledges the financial support of the National Key R&D Program of China (No. 2017YFB0701604). XY acknowledges the financial support of National Natural Science Foundation of China Projects (No. 51701171), and a research grant from the Hong Kong Polytechnic University (1-99QP).

Reference

[1] S. Hao, L. Cui, D. Jiang, X. Han, Y. Ren, J. Jiang, Y. Liu, Z. Liu, S. Mao, Y. Wang, Y. Li, X. Ren, X. Ding, S. Wang, C. Yu, X. Shi, M. Du, F. Yang, Y. Zheng, Z. Zhang, X. Li, D.E.

Brown, J. Li, A Transforming Metal Nanocomposite with Large Elastic Strain, Low Modulus, and High Strength, Science (80-.). 339 (2013) 1191–1194.

[2] Z. Li, K.G. Pradeep, Y. Deng, D. Raabe, C.C. Tasan, Metastable high-entropy dual-phase alloys overcome the strength–ductility trade-off, Nature. 534 (2016) 227–230.

[3] D. Wang, Y. Wang, Z. Zhang, X. Ren, Modeling Abnormal Strain States in Ferroelastic Systems: The Role of Point Defects, Phys. Rev. Lett. 105 (2010) 205702.

[4] X. Ren, Strain Glass and Strain Glass Transition, in: T. Kakeshita, T. Fukuda, A. Saxena, A. Planes (Eds.), Disord. Strain-Induced Complex. Funct. Mater., Springer, Berlin, 2012: pp. 201–225.

[5] Y. Song, X. Chen, V. Dabade, T.W. Shield, R.D. James, Enhanced reversibility and unusual microstructure of a phase-transforming material, Nature. 502 (2013) 85–8.

[6] J. Cui, Y.S. Chu, O.O. Famodu, Y. Furuya, J. Hattrick-Simpers, R.D. James, A. Ludwig, S. Thienhaus, M. Wuttig, Z. Zhang, I. Takeuchi, Combinatorial search of thermoelastic shape-memory alloys with extremely small hysteresis width, Nat. Mater. 5 (2006) 286–290.

[7] C. Chluba, H. Ossmer, C. Zamponi, M. Kohl, E. Quandt, Ultra-Low Fatigue Quaternary TiNi-Based Films for Elastocaloric Cooling, Shape Mem. Superelasticity. 2 (2016) 95–103.

[8] Z. Zhang, X. Ding, J. Sun, T. Suzuki, T. Lookman, K. Otsuka, X. Ren, Nonhysteretic Superelasticity of Shape Memory Alloys at the Nanoscale, Phys. Rev. Lett. 111 (2013) 145701.

[9] A. Ahadi, Q. Sun, Stress-induced nanoscale phase transition in superelastic NiTi by in situ X-ray diffraction, Acta Mater. 90 (2015) 272–281.

[10] J. Zhu, Y. Gao, D. Wang, J. Li, T.-Y. Zhang, Y. Wang, Making metals linear super-elastic with ultralow modulus and nearly zero hysteresis, Mater. Horizons. 6 (2019) 515–523.

[11] M. Geetha, A.K. Singh, R. Asokamani, A.K. Gogia, Ti based biomaterials, the ultimate choice for orthopaedic implants – A review, Prog. Mater. Sci. 54 (2009) 397–425.

[12] J. Mohd Jani, M. Leary, A. Subic, M.A. Gibson, A review of shape memory alloy research, applications and opportunities, Mater. Des. 56 (2014) 1078–1113.

[13] K.T. Park, M. Esashi, Multilink active catheter with polyimide-based integrated CMOS interface circuits, J. Microelectromechanical Syst. 8 (1999) 349–357.

[14] X. Moya, S. Kar-Narayan, N.D. Mathur, Caloric materials near ferroic phase transitions, Nat. Mater. 13 (2014) 439–50.

[15] H.-H. Wu, J. Zhu, T.-Y. Zhang, Pseudo-first-order phase transition for ultrahigh positive/negative electrocaloric effects in perovskite ferroelectrics, Nano Energy. 16 (2015) 419–427.

[16] S. Sarkar, X. Ren, K. Otsuka, Evidence for Strain Glass in the Ferroelastic-Martensitic System Ti50−xNi50+x, Phys. Rev. Lett. 95 (2005) 205702.

[17] J. Zhu, Y. Gao, D. Wang, T.-Y. Zhang, Y. Wang, Taming martensitic transformation via concentration modulation at nanoscale, Acta Mater. 130 (2017) 196–207.

[18] D.L. Moffat, U.R. Kattner, The stable and metastable Ti-Nb phase diagrams, Metall. Trans. A. 19 (1988) 2389–2397.

[19] O. Lyon, C. Severac, C. Servant, Spinodal decomposition and isothermal ω-phase formation in a Ti-Nb alloy, investigated by small-angle X-ray scattering, Philos. Mag. A. 48 (1983) 825–839.

[20] K. Tsuchiya, H. Sato, S. Edo, K. Marukawa, M. Umemoto, Effect of aging on martensitic transformation in γ-MnCu alloy, Mater. Sci. Eng. A. 285 (2000) 353–356.

[21] F. Yin, Y. Ohsawa, A. Sato, K. Kawahara, Phase decomposition of the γ phase in a Mn–30 at.% Cu alloy during aging, Acta Mater. 48 (2000) 1273–1282.

[22] F. Findik, Improvements in spinodal alloys from past to present, Mater. Des. 42 (2012) 131–146.

[23] Y.L. Hao, H.L. Wang, T. Li, J.M. Cairney, A.V. Ceguerra, Y.D. Wang, Y. Wang, D. Wang, E.G. Obbard, S.J. Li, R. Yang, Superelasticity and Tunable Thermal Expansion across a Wide Temperature Range, J. Mater. Sci. Technol. 32 (2016) 705–709.

[24] J. Liu, Y.Y. Wang, Y.-L. Hao, Y.Y. Wang, Z. Nie, D. Wang, Y. Ren, Z. Lu, J. Wang, H. Wang, X. Hui, N. Lu, M.J. Kim, R. Yang, New intrinsic mechanism on gum-like superelasticity of multifunctional alloys, Sci. Rep. 3 (2013) 2156.

[25] J. Zhu, H. Wu, D. Wang, Y. Gao, H. Wang, Y. Hao, R. Yang, T.-Y. Zhang, Y. Wang, Crystallographic analysis and phase field simulation of transformation plasticity in a multifunctional β-Ti alloy, Int. J. Plast. 89 (2017) 110–129.

[26] L.D. Landau, E.M. Lifshitz, Statistical physics, Pergamon Press, Oxford, 1980.

[27] J.W. Cahn, J.E. Hilliard, Free Energy of a Nonuniform System. I. Interfacial Free Energy, J. Chem. Phys. 28 (1958) 258.

[28] J.W. Cahn, Free Energy of a Nonuniform System. II. Thermodynamic Basis, J. Chem. Phys. 30 (1959) 1121–1124.

[29] A.G. Khachaturyan, Theory of Structural Transformations in Solids, John Wiley & Sons, New York, 1983.

[30] J. Zhu, T. Zhang, Y. Yang, C.T. Liu, Phase field study of the copper precipitation in Fe-Cu alloy, Acta Mater. 166 (2019) 560–571.

[31] J. Cahn, On spinodal decomposition, Acta Metall. 9 (1961) 795–801.

[32] J.D. Gunton, M.S. Miguel, P.S. Sahni, The Dynamics of First Order Phase Transitions, in: E.C. Domb, J. Lebowitz (Eds.), Phase Transitions Crit. Phenom., Academic Press, London, 1983: pp. 269–466.

[33] G.B. Olson, M. Cohen, A general mechanism of martensitic nucleation: Part I. General concepts and the FCC → HCP transformation, Metall. Trans. A. 7 (1976) 1897–1904.

[34] G.B. Olson, M. Cohen, A general mechanism of martensitic nucleation: Part II. FCC → BCC and other martensitic transformations, Metall. Trans. A. 7 (1976) 1905–1914.

[35] J. Frenzel, A. Wieczorek, I. Opahle, B. Maaß, R. Drautz, G. Eggeler, On the effect of alloy composition on martensite start temperatures and latent heats in Ni–Ti-based shape memory alloys, Acta Mater. 90 (2015) 213–231.

[36] Y.A. Chu, B. Moran, G.B. Olson, A.C.E. Reid, A model for nonclassical nucleation of solid-solid structural phase transformations, Metall. Mater. Trans. A. 31 (2000) 1321–1331.

[37] H.Y. Yu, S.C. Sanday, B.B. Rath, On the heterogeneous nucleation of martensite, Mater. Sci. Eng. B. 32 (1995) 153–158.

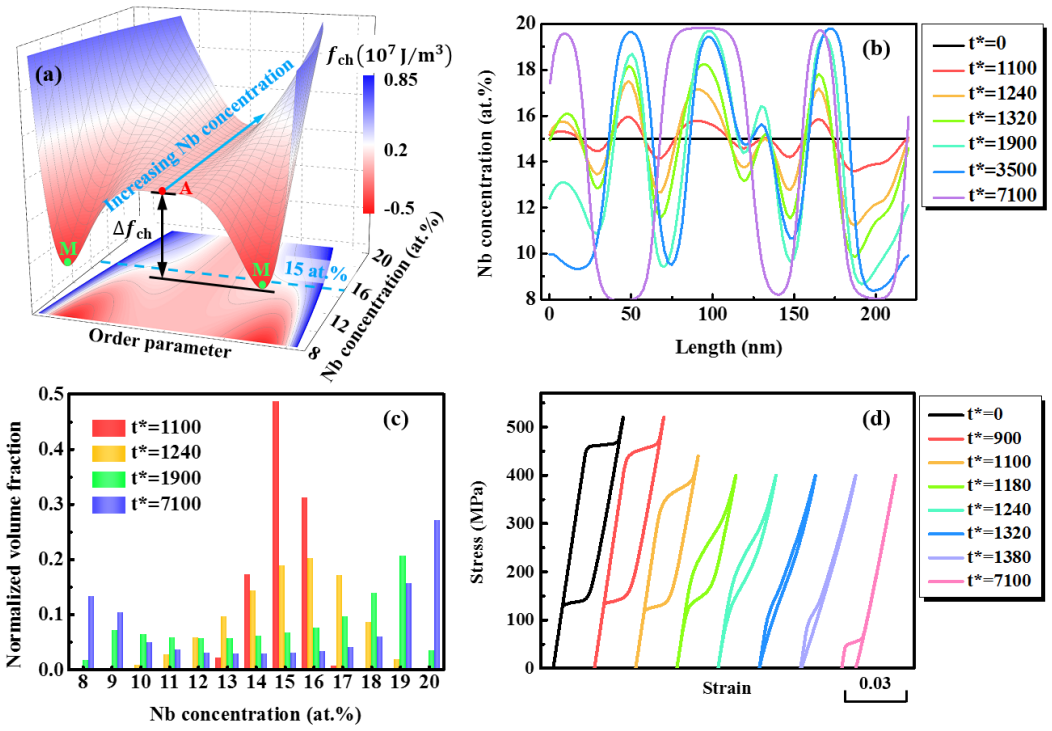

Fig. 1 (a) Landau free energy surface that characterizes the concentration dependence of chemical free energy of austenites and martensites. Letters A and M represent austenite and martensite, respectively. The difference in chemical free energy between austenite and martensite is defined as chemical driving force of MT, i.e. $\Delta f_{\mathrm{ch}} = f_{\mathrm{ch}}(\mathrm{Martensite}) - f_{\mathrm{ch}}(\mathrm{Austenite})$. The blue dashed line denotes the initial concentration of the system before spinodal decomposition. (b) One-dimensional Nb concentration profiles along the body-diagonal of the three-dimensional computation cell aged for different times during spinodal decomposition. (c) Statistical distributions of voxels having certain Nb concentration in the computational cell aged for different time. (d) SS curves of systems aged for different time.

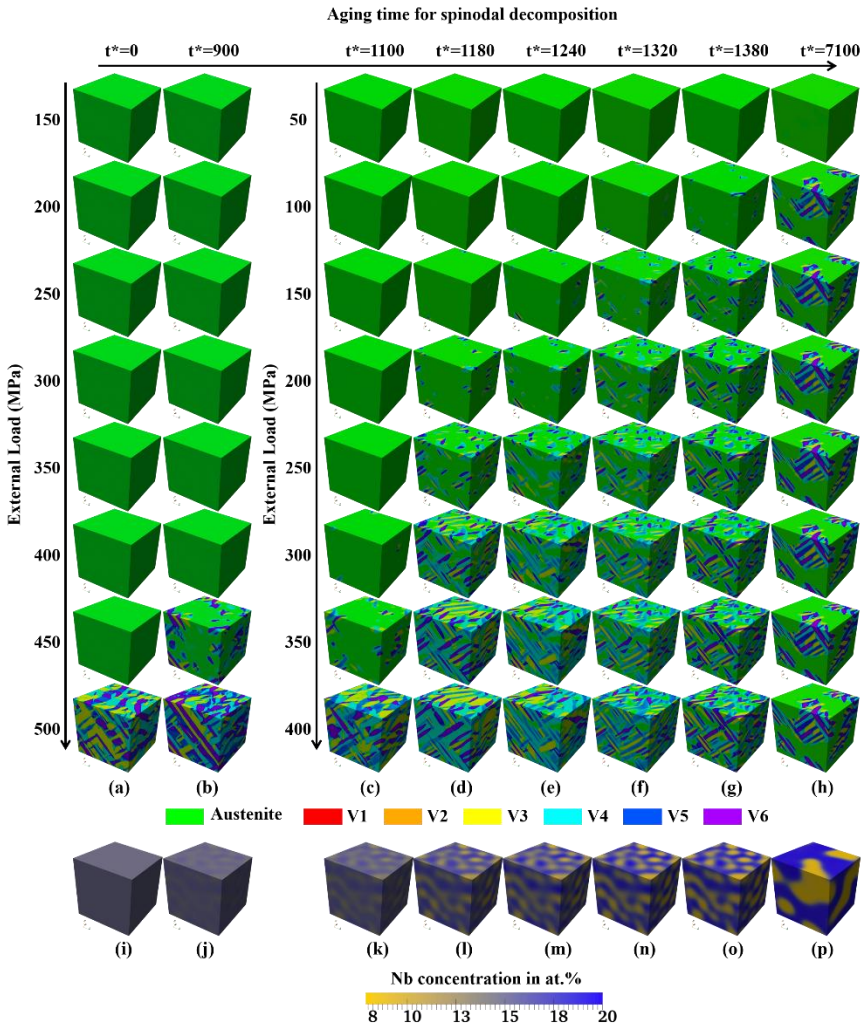

Fig. 2. (a)-(h) Microstructure evolution of systems aged for different time upon loading. Austenite and six martensitic variants (V1~V6) are represented by different colors as indicated at the bottom. (i)-(p) Nb CM generated from spinodal decomposition in the parent phase by ageing different time at 773K.

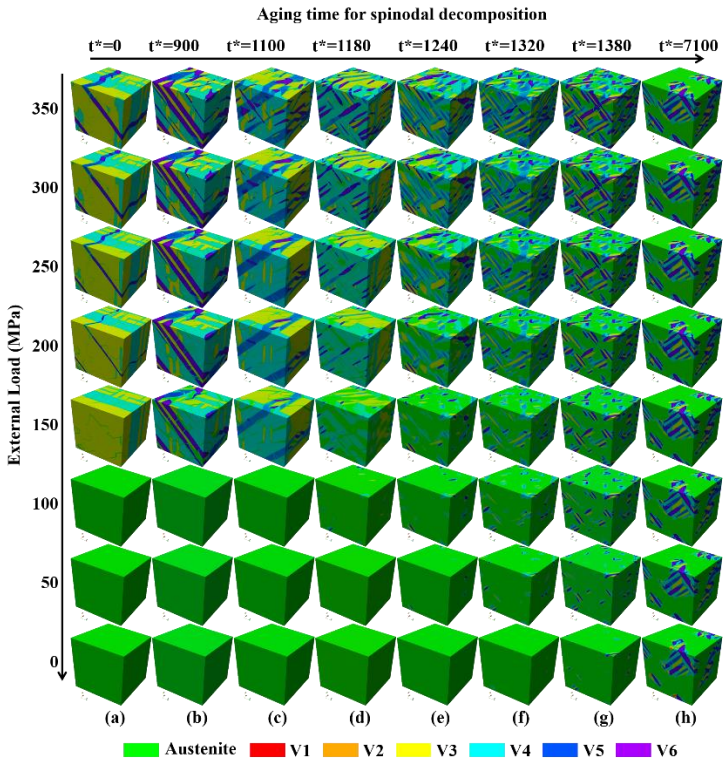

Fig. 3. Microstructure evolution of systems aged for different time upon unloading. Austenite and six martensitic variants (V1~V6) are represented by different colors as indicated at the bottom.

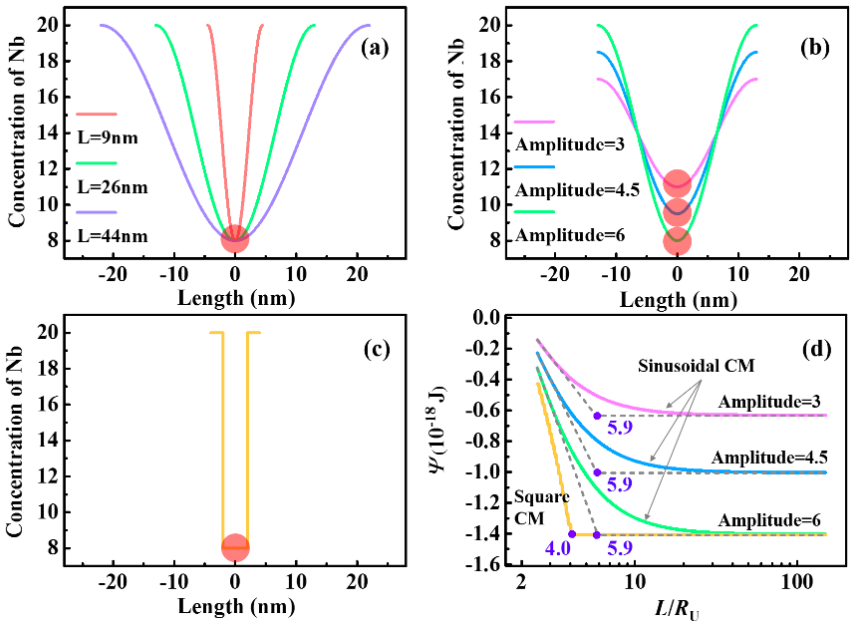

Fig. 4. (a) and (b) show CMs with different wavelength and amplitude, respectively. (c) plots a square CM. Red spheres in (a)-(c) indicate the sphere over which the integration of Eq. (2) is performed. (d) shows the variation of Ψ with normalized CM wavelength, i.e. L/R_{U}, in sinusoidal and square CMs. $\Psi = \Delta F_{\mathrm{ch}}^{\mathrm{CM}} - \Delta F_{\mathrm{ch}}^{\mathrm{U}}$ is defined as the difference in chemical driving force before ($\Delta F_{\mathrm{ch}}^{\mathrm{U}}$) and after ($\Delta F_{\mathrm{ch}}^{\mathrm{CM}}$) introducing CM.

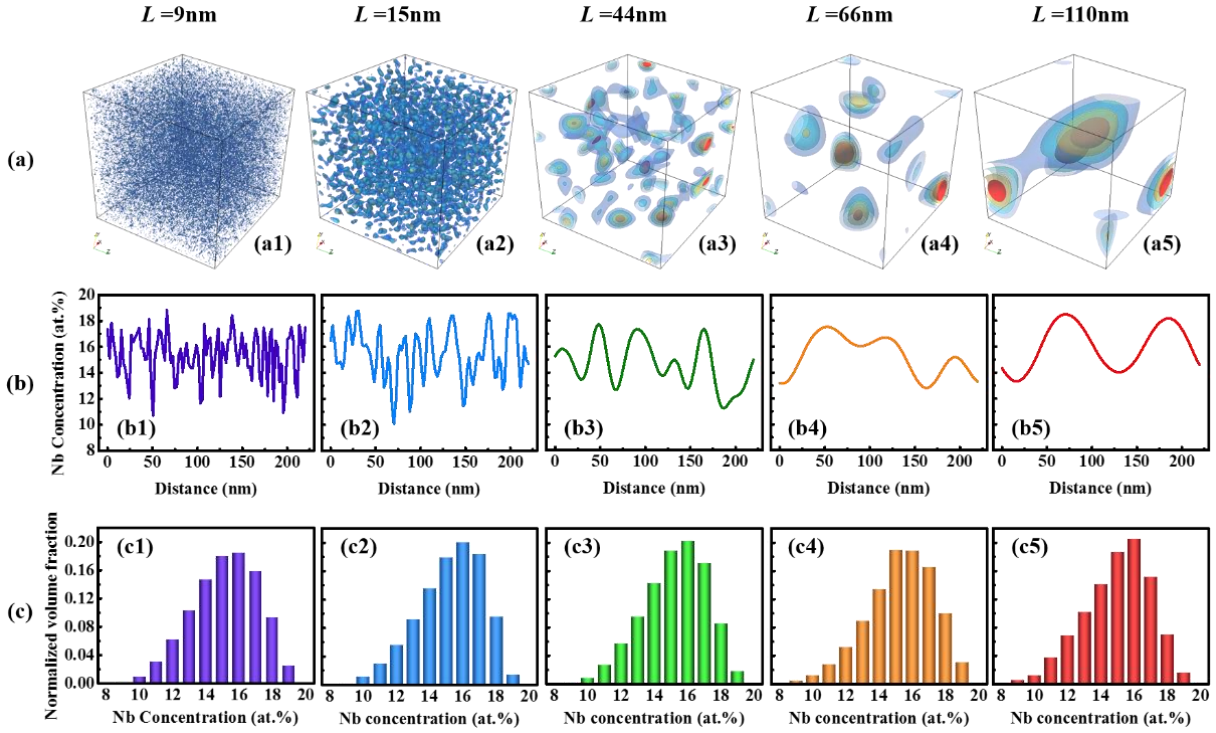

Fig. 5. (a1)-(a5) show 3D CMs of different wavelengths. Semi-transparent iso-surfaces are used to represent Nb concentrations of 9.3, 10, 11, and 12 at.%. (b1)-(b5) show the concentration variation of Nb along one body diagonal of computational cells shown in (a1)-(a5). (c1)-(c5) are statistical distributions of Nb concentration in systems shown in (a1)-(a5).

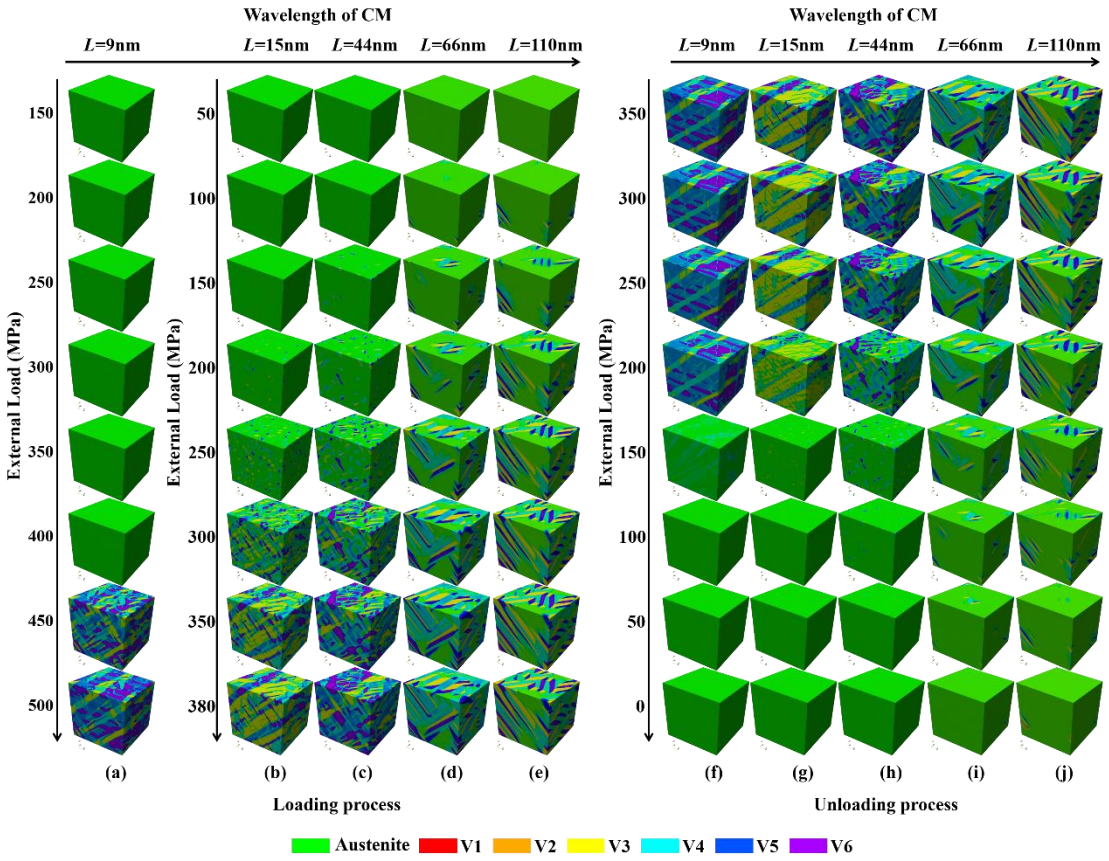

Fig. 6. Microstructure evolution of systems with different concentration wavelength during (a)-(e) loading and (f)-(j) unloading process. Austenite and six martensitic variants are represented by different colors as indicated at the bottom.

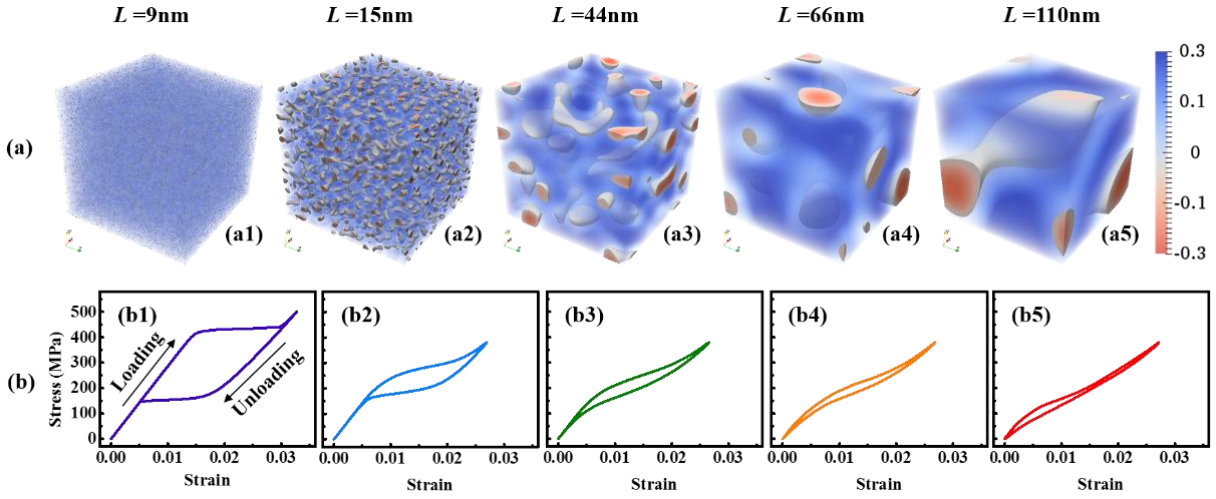

Fig. 7. (a1)-(a5) show chemical driving force, Δf_{ch}, of systems presented in Fig. 5(a) without applying external load. (b1)-(b5) are the uniaxial loading SS curves of these systems.

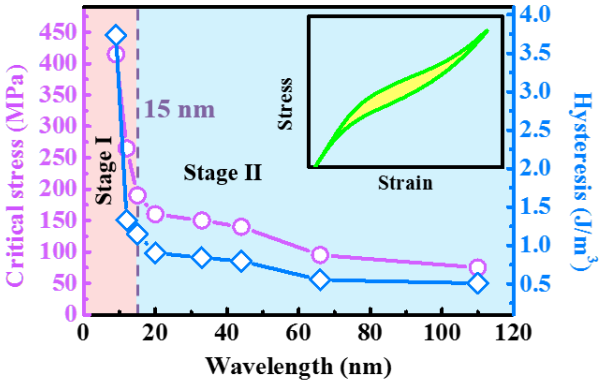

Fig. 8. Variation of σ_{M_s} and hysteresis with CM wavelength. The hysteresis is defined as the area enclosed by the SS curve as the inset shows.

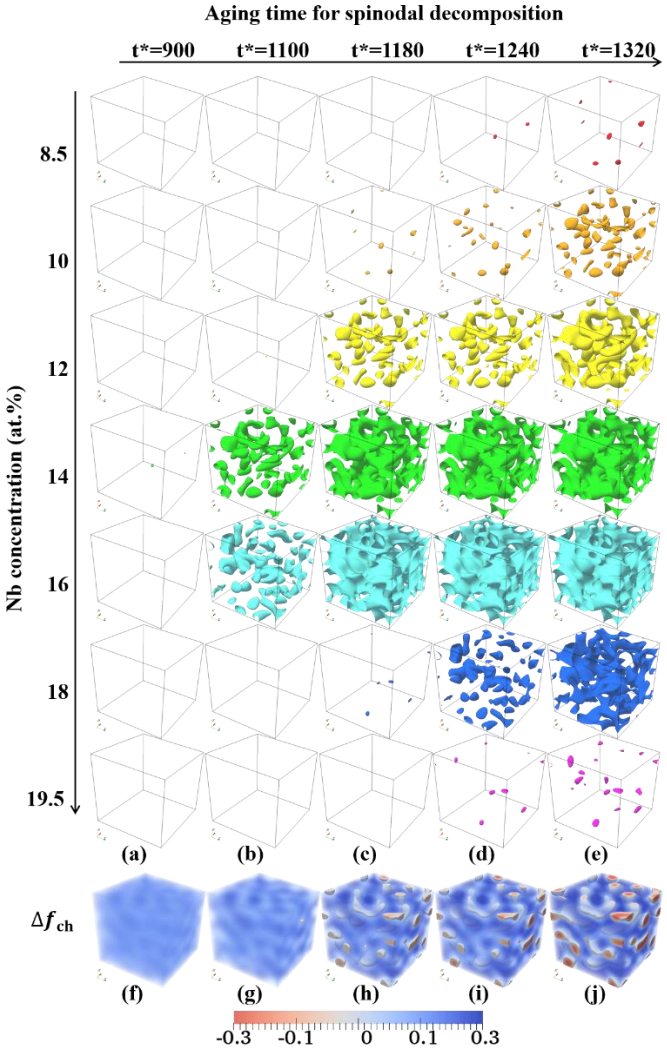

Fig. 9. (a)-(e) Morphology of representative concentrations in systems aged for different time during spinodal decomposition. Different Nb concentrations are represented by iso-surfaces with different colors in each system. (f)-(j) Driving force of MT, Δf_{ch}, in systems aged for different time without applying external load. A negative driving force, Δf_{ch} <0, is required for forward MT.

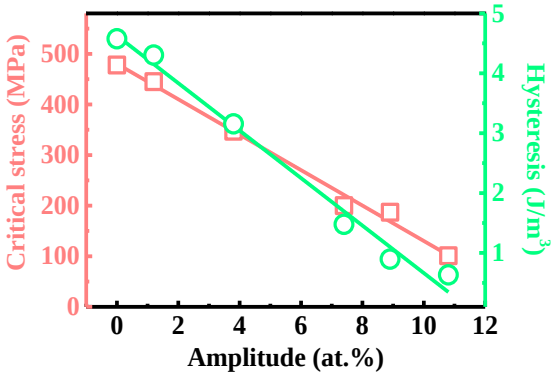

Fig. 10. Variation of σ_{M_s} and hysteresis with CM amplitude. The open symbols represent results obtained from quantitative analyses on SS curves (t*=0-1320) shown in Fig. 1(d) and the solid lines are drawn to guide the eyes.

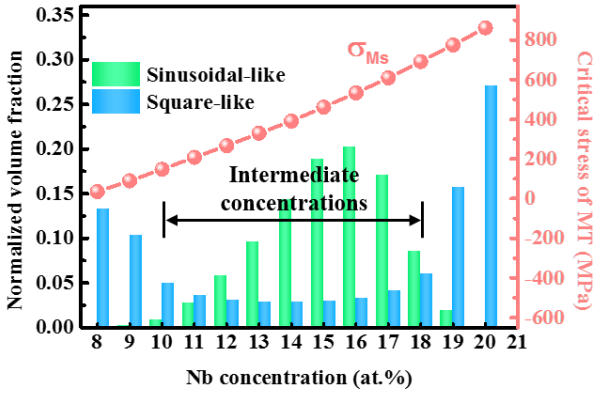

Fig. 11. Statistical distribution of concentration of CMs with sinusoidal-like and square-like concentration profiles. The sinusoidal-like and square-like CMs correspond to systems shown in Fig. 2(m) and (p). The red line shows the σ_{M_s} of different concentrations.

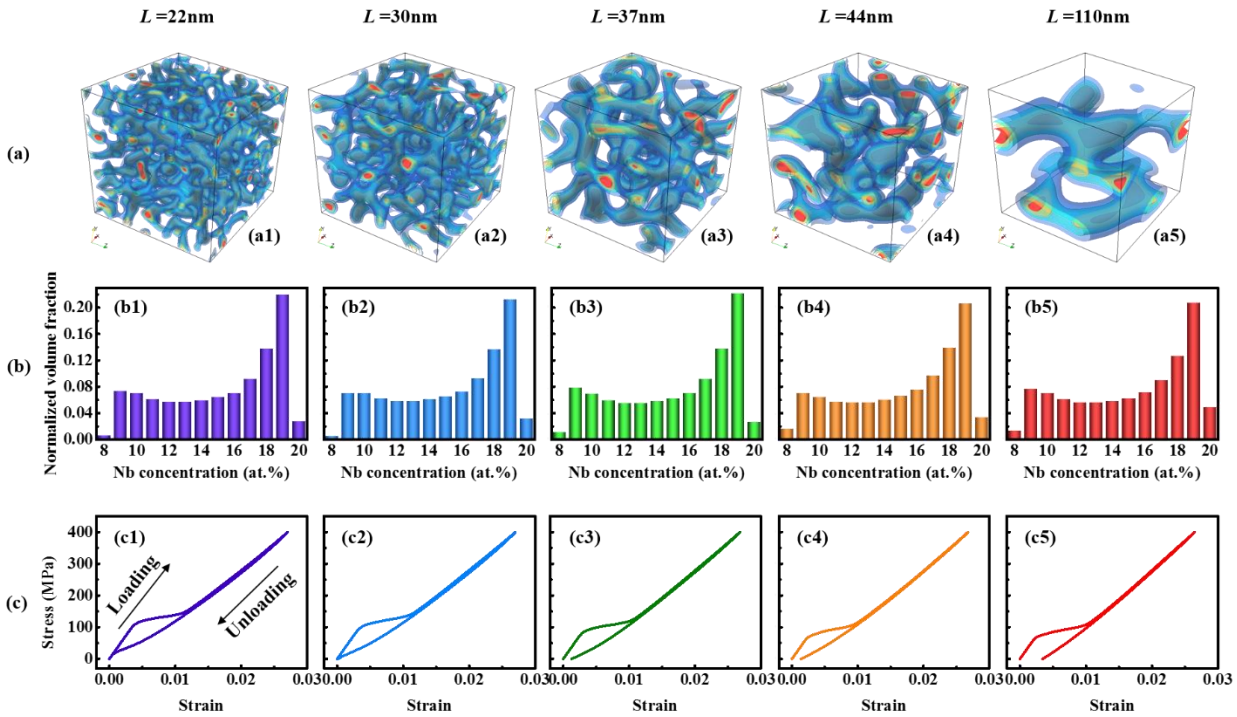

Fig. 12. (a1)-(a5) Systems with square-like CMs of different wavelengths. The representative semi-transparent iso-surfaces have Nb concentrations of 9.3, 10, 11, and 12 at.%, respectively. Statistical distributions of Nb concentration of these systems are shown in (b1)-(b5). SS curves of these systems under uniaxial loading are plotted in (c1)-(c5).

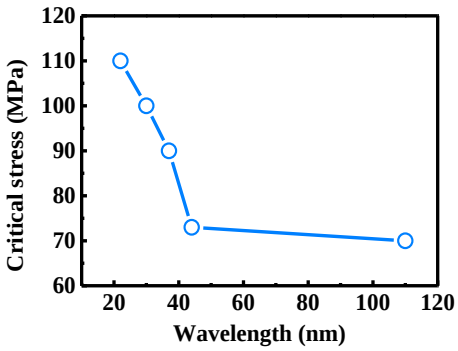

Fig. 13. Variation of σ_{M_s} with CM wavelength in systems shown in Fig. 12.